Improved Ru/Si multilayer reflective coatings for advanced extreme ultraviolet lithography photomasks

Obert Wood[*1], Keith Wong[1], Valentin Parks[1], Patrick Kearney[2], Julia Meyer-Ilse[3], Vu Luong[4], Vicky Philipsen[4], Mohammad Faheem[1], Yifan Liang[1], Ajay Kumar[1], Esther Chen[1], Corbin Bennett[1], Bianzhu Fu[1], Michael Gribelyuk[1], Wayne Zhao[1], Pawitter Mangat[1], Paul van der Heide[1]

[1]GLOBALFOUNDRIES, 400 Stonebreak Rd. Extension, Malta, NY 12020 USA
[2]SUNY Poly SEMATECH, 257 Fuller Road, Albany, NY 12203 USA
[3]Lawrence Berkeley National Laboratory, 1 Cyclotron Road, Berkeley, CA 94720 USA
[4]IMEC, Kapeldreef 75, B-3001 Leuven, Belgium

ABSTRACT

Extreme ultraviolet (EUV) lithography with reflective photomasks continues to be a potential patterning technology for high volume manufacturing at the 7 nm technology node and beyond. EUV photomasks with alternative materials to the commonly used Mo/Si multilayer (ML) reflector and patterned Ta-based absorber (both of which are known to require shadow effect corrections and lead to large through-focus pattern placement errors) are being actively explored. Because the reflective bandwidth of a Ru/Si ML is significantly wider than the reflective bandwidth of a Mo/Si ML and the effective reflectance plane in Ru/Si is closer to the ML surface, Ru/Si ML coatings may be viable alternatives to the Mo/Si ML coatings that are commercially available today because they will lead to smaller mask 3D effects. In this paper, increases in the peak reflectivity and the reflective bandwidth of Ru/Si ML reflectors by using B_4C interlayers to improve the Ru-Si interfaces are discussed. The conclusions of this paper are supported with the results of both experimental measurements and rigorous simulations.

Keywords: EUV, EUV mask, mask stack, Ru/Si ML reflector, B_4C interlayers, rigorous 3D lithography simulation.

1. INTRODUCTION

All extreme ultraviolet masks are comprised of a multilayer film stack, which ideally provides a high reflectivity for all occurring angles of incidence, and a patterned absorber or shifter layer, which defines the features on the mask. Because EUV reflective masks are illuminated at an oblique angle in order to separate incident and reflected light, their coating structure has an inordinately large impact on image quality and gives rise to a horizontal-vertical print difference due to mask shadowing and through-focus pattern placement errors that vary dramatically with pattern pitch [1,2]. If multiple patterning 193-nm immersion lithography at the 7 nm and lower technology nodes is to be replaced with single-exposure EUV lithography, then EUV projection optics with higher than 0.33 NA, more extreme off-axis illumination schemes, and/or masks with smaller 3D effects will be needed. In this paper, the performance of masks with Ru/Si ML reflective coatings [3.4] instead of the commonly used Mo/Si ML reflector is discussed. In Section 2.1, the current performance and some of the potential advantages of Ru/Si ML reflective coatings are summarized. In Section 2.2, recent improvements in Ru/Si ML performance with B_4C interlayers are described. In Section 2.3, a model of a Ru/Si ML with B_4C interlayers that can be used to accurately simulate the imaging performance of Ru/Si ML coatings in EUV scanners at 0.33 and 0.55 NA is presented. In Section 3, the results of rigorous simulations of various lithography performance parameters and the magnitude of 3D effects such as mask shadowing and telecentricity errors are presented. In Section 4 the main findings of the paper are summarized and some suggestions for future work are provided.

[*] obert.wood@globalfoundries.com; phone 1 518 305-7809

2. RUTHENIUM-SILICON MULTILAYER REFLECTIVE COATINGS

2.1 Current Statue of Ru/Si ML Coatings

EUV reflectivity versus wavelength and EUV reflectivity versus angle of incidence for ideal Mo/Si and Ru/Si multilayers (no intermixing at the interfaces) using constants for Mo, Ru, and Si from the CXRO website [5] are shown in Fig. 1.

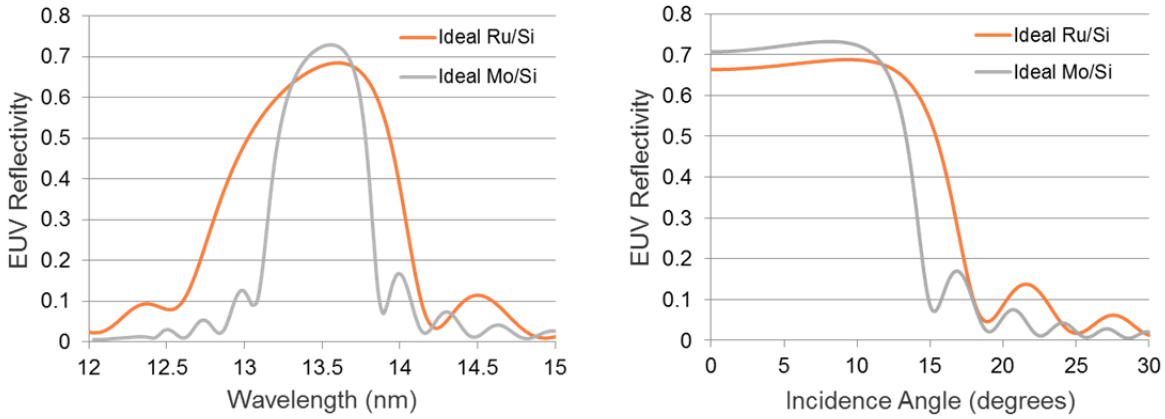

Figure 1 Left: Plots of reflectivity versus EUV wavelength at 6° angle of incidence for an ideal Mo/Si ML with 40 bilayers (in grey) and an ideal Ru/Si ML with 20 bilayers (in red). Right: Plots of EUV reflectivity versus incident angle at 13.5 nm wavelength for an ideal Mo/Si ML with 40 bilayers (in grey) and an ideal Ru/Si ML with 20 bilayers (in red).

Due to the lower index of refraction of Ru compare to Mo, the spectral bandwidth of Ru/Si MLs is predicted to be significantly broader than that of Mo/Si MLs. The Ru/Si ML design saturates at a lower reflectivity than its Mo/Si counterpart because of the higher extinction coefficient of Ru compared to Mo. For this reason Ru/Si ML coatings have not normally been used on the reflective optics in EUV exposure tools. The higher extinction coefficient of Ru compare to Mo also causes the Ru/Si ML design to saturate with a smaller number of bilayers (~ 33) than its Mo/Si ML counterpart (~ 40) as shown in Fig. 2 (left) and, hence, Ru/Si ML coatings should potentially have lower defectivity.

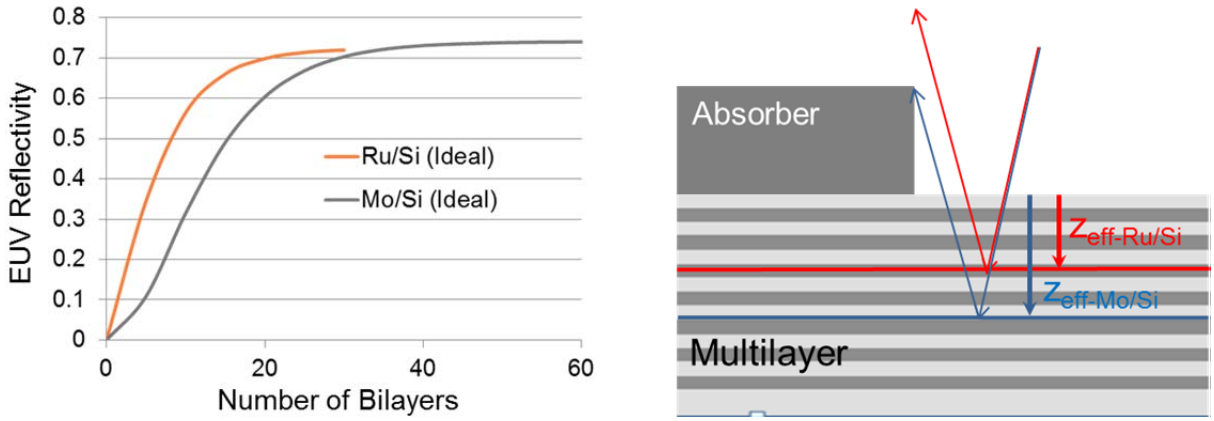

Figure 2 Left: Plots of reflectivity at 13.5 nm wavelength and 6° angle of incidence versus the number of bilayers for an ideal Ru/Si ML (in red) and an ideal Mo/Si ML (in grey). Right: Cross section of an EUV mask stack illustrating the relative position of the effective reflectance plane (Z_{eff}) in Ru/Si and Mo/Si ML coatings: Z_{eff} ~ 33 nm in Ru/Si and Z_{eff} ~ 45 nm in Mo/Si. Note: the multilayer period shown schematically is not to scale.

Because of the lower index of refraction of Ru compared to Mo, the phase change upon reflection in Ru/Si exhibits a shallower gradient causing the effective reflectance plane in Ru/Si ML coatings to be ~10-15 nm closer to the coating

surface, as shown in Fig. 2 (right). The results presented in this paper suggest that the use of Ru/Si ML coatings on EUV masks could lead to smaller mask 3D effects, i.e., less mask shadowing and smaller pattern placement (telecentricity) errors. Plots of EUV reflectivity versus wavelength at 6° angle of incidence and EUV reflectivity versus incident angle at 13.5 nm wavelength for ideal and state-of-the-art Ru/Si MLs with 20 bilayers are shown in Figure 3.

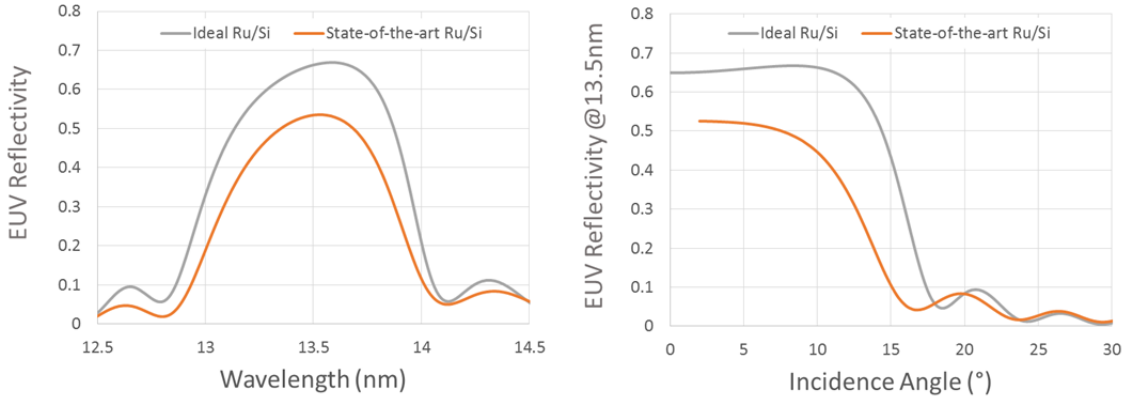

Figure 3 Left: Plots of EUV reflectivity versus wavelength at 6° angle of incidence for ideal (grey) and state-of-the-art Ru/Si MLs with 20 bilayers (red). Right: Plots of EUV reflectivity versus incident angle at 13.5 nm wavelength for ideal (grey) and state-of-the-art Ru/Si MLs with 20 bilayers (red).

The comparisons of the reflectivity performance of ideal and state-of-the-art Ru/Si MLs shown in Figure 3 suggests that considerable improvements in the peak EUV reflectivity and the reflective bandwidth of Ru/Si MLs should be possible by employing interface engineering with C [6] or B_4C [7,8] interlayers to sharpen the interfaces.

2.2 Improvements in Ru/Si ML Coatings with B_4C Interlayers

Just as is the case with the Mo/Si ML coatings that are present on the majority of all EUV reflective optics today, the width and roughness of the Ru-Si ML interfaces play a large role in determining the performance of Ru/Si ML coatings [7]. In this work, information on Ru-Si interfaces was obtained by depositing Ru/Si ML coatings with a variety of different coating designs on silicon wafers and measuring reflectivity versus wavelength and reflectivity versus angle of incidence in the EUV spectral region, collecting XTEM images of the films, and by matching simulation to experimental data. All of the Ru/Si ML coatings used in this work were deposited in low pressure Ar gas using a PVD tool. The Ru/Si test samples had different values for the total bilayer thickness, gamma values of 0.4 (where gamma is the fraction of the bilayer occupied by Ru), and with a variety of B_4C-interlayer thicknesses from 0 – 20 Å to retard interlayer diffusion and improve the Ru/Si interfaces. All of the Ru/Si coatings were designed to have a Si layer at the bottom of the film and a Ru layer at the top of the film, to have a multilayer period of ~7 nm to provide a maximum reflectivity at 13.5 nm wavelength at 6 degrees incident angle, and to have a total of 20 bilayers.

X-ray reflectometry (XRR) was used to determine the Ru/Si bilayer period of the coatings on the test samples [9]. An example of an XRR spectrum recorded from a Ru/Si ML-coated sample with 20 bilayers is shown in Figure 4 (left). A plot of *Slope* determined from a plot of *sin(Radian(2Theta/2)^2* versus *Order^2* from the XRR data shown in Figure 4 (left) is shown in Figure 4 (right). The value of *Slope* can be used in Equation 1 to determine the ML period with sub-Å accuracy because of the extensive averaging involved.

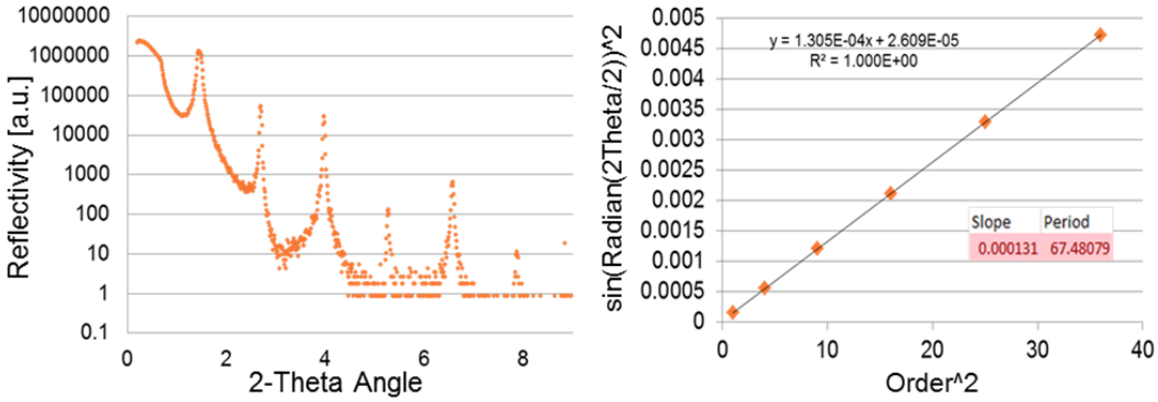

Figure 4 Left: Plot of x-ray reflectivity (XRR) at 1.54060 Å wavelength versus 2-Theta Angle from a silicon wafer coated with 20 bilayers of Ru and Si. Right: X-ray reflectivity data plotted as *sin(Radian(2Theta/2))^2* versus *Order^2* which can be used in Equation 1 to accurately determine the ML Period.

$$\text{ML Period} = \frac{\lambda/2}{\sqrt{Slope}} \quad \text{where } \lambda = 1.54060 \text{ Å} \tag{1}$$

More than 20 Si wafers were coated with Ru/Si ML films with B_4C interlayers at various thickness from 0 to 20 Å. For these samples ML Period Contraction values were determined from Equation 2 using the known thickness of Ru, B_4C and Si deposited layers and the measured ML Period values.

$$\text{ML Period Contraction} = \text{ML Period (Measured)} + T_{Ru} + T_{B4C} + T_{Si} \tag{2}$$

If no B_4C interlayers were present and no interdiffusion of the Ru and Si layers took place or no compounds (silicides) were formed then there would be no significant period contraction. In such cases the interfaces between Ru and Si would be narrow and the synthetic Bragg reflectivity of the resulting film would be expected to be high. In films in which B_4C interlayers were present, the B_4C thickness values that resulted in the lowest values of ML Period Contraction were found to correspond to coatings with the highest peak EUV reflectivity and widest EUV reflective bandwidth. Then, according to the data plotted in Figure 5, the optimum B_4C interlayer films should be approximately 10 Å thick.

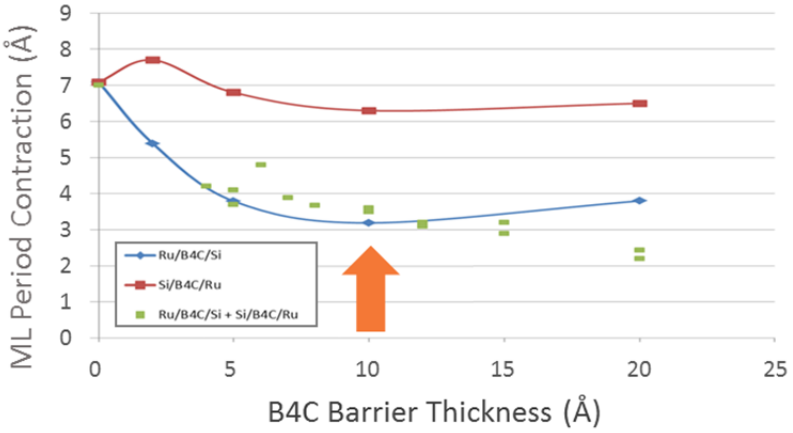

Figure 5 Plot of ML Period Contraction versus B_4C barrier thickness for both types of Ru-Si interfaces, i.e., with B_4C films deposited on top of the Si layers and with B_4C layers deposited on top of the Ru layers showing that the optimum B_4C barrier thicknesses in both cases are approximately 10 Å.

Plots of measured reflectivity versus EUV wavelength and EUV reflectivity versus angle of incidence of a Ru/Si ML coating with 20 bilayers with and without 10 Å thick B_4C interlayers at both types of Ru-Si interfaces are shown in Figure 6.

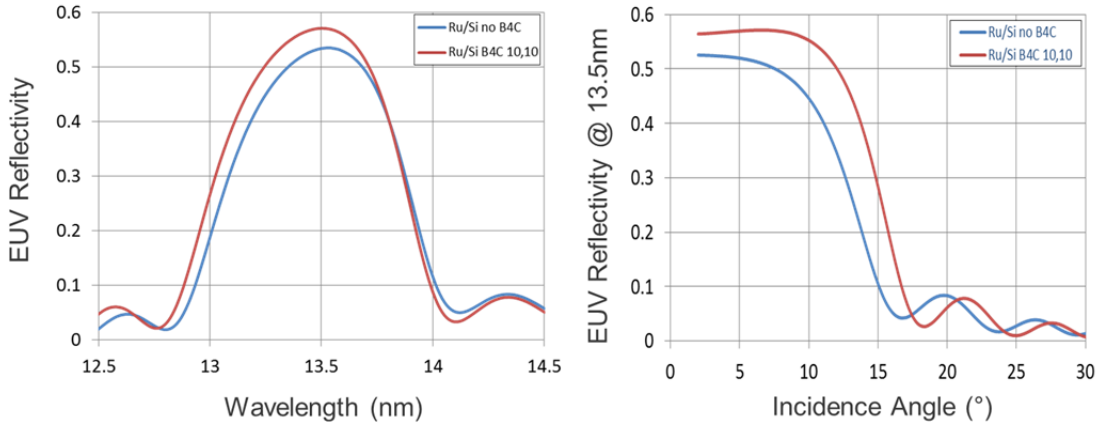

Figure 6 Plots of measured EUV reflectivity versus wavelength and EUV reflectivity at 13.5 nm wavelength versus angle of incidence of a 20 bilayers Ru/Si ML coated sample with and without 10 Å thick B_4C interlayers.

Peak reflectivity and reflective bandwidth of the Ru/Si ML with B_4C interlayers have clearly been improved but coating performance is still dominated by interdiffusion.

2.3 Development of Ru/Si ML with B_4C Interlayer Model

Electron energy loss spectra (EELS) collected from a sample of Ru/Si ML with 10 Å thick B_4C interfaces deposited on both types of Ru-Si interfaces are shown in Figure 7.

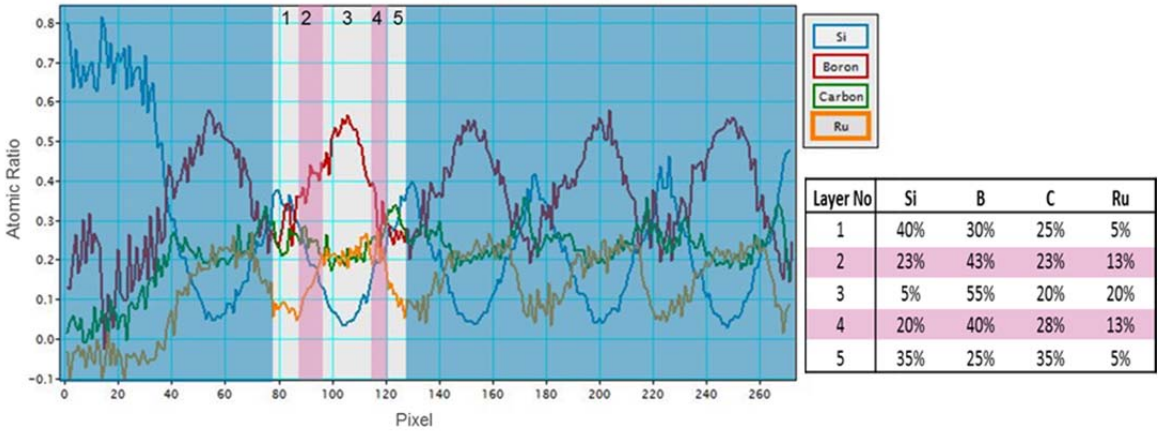

Layer No	Si	B	C	Ru
1	40%	30%	25%	5%
2	23%	43%	23%	13%
3	5%	55%	20%	20%
4	20%	40%	28%	13%
5	35%	25%	35%	5%

Figure 7 Left: Plots of EELS profiles for Silicon, Boron, Carbon and Ruthenium from a silicon wafer coated with a Ru/Si ML with 10 Å thick B_4C interlayers as a function of film height (the Si wafer is located at the left). Right: Table listing the percentage of Si, B, C and Ru present in each of the 5 distinct layers that can be identified within each Ru-Si period.

Measurements of reflectivity versus wavelength and reflectivity at 13.5 nm wavelength versus angle of incidence for a 20 bilayer Ru/Si coated sample with 10 Å thick B_4C interlayers at each type of interface, carried out using the EUV Standards and Calibration beamline at the Advanced Light Source in Berkeley, are shown in Figure 8 (solid curves).

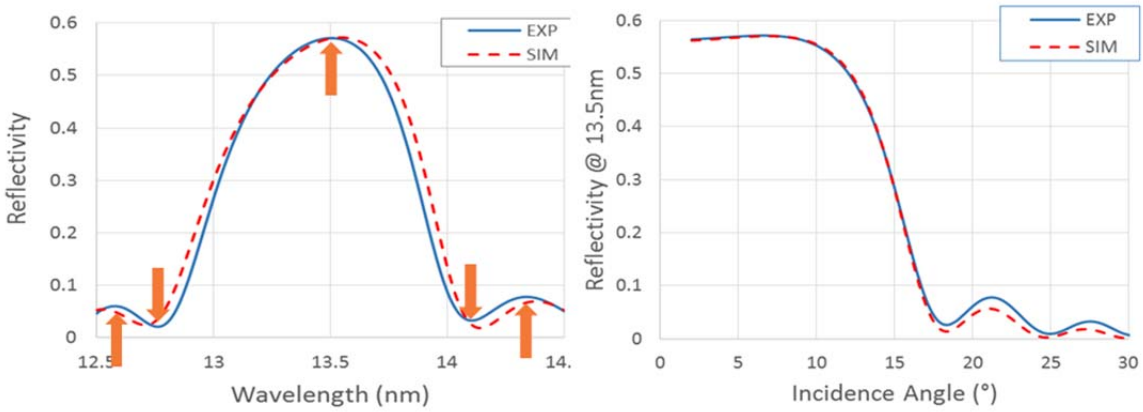

Figure 8 Comparison of measured and simulated reflectivity versus wavelength (left) and reflectivity at 13.5 nm wavelength versus incident angle (right) showing that reasonable agreement between measured and simulated UV reflectivity can be obtained with a 5 layer model for each Ru/Si period.

The simulations of measured and simulated reflectivity versus wavelength and reflectivity at 13.5 nm wavelength shown in Figure 8 (dashed curves) were obtained with a model based on the input parameters listed in Table 1. The measured reflectivity versus wavelength data shown in Figure 8 were fitted at the 5 wavelengths indicated with arrows with SLitho Software using the thickness values and atomic ratios determined from the EELS spectra shown in Figure 7 and by allowing the thickness of the top-most layers and the densities of the 5 distinct layers in each Ru/Si bilayer period to vary. The fitted densities of the compounds were constrained be less than those of the pure materials. The optimum density values determined as a result of the SLitho [10] fitting are listed in Table 1 (on the right).

Layer	Compound	Period Thickness [Å]	Top Thickness [Å]	Density [g/cm³]	n @ 13.5nm	k @ 13.5nm
3	Si1_B11_C4_Ru4		61			
2	Si9_B17_C9_Ru5		4.1			
1	Si8_B6_C5_Ru1		3.4			
5	Si7_B5_C7_Ru1	9.9		0.66	0.995	-0.001
4	Si8_B16_C11_Ru5	8.6		2.66	0.976	-0.004
3	Si1_B11_C4_Ru4	23.9		11	0.887	-0.017
2	Si9_B17_C9_Ru5	15.8		0.66	0.994	-0.001
1	Si8_B6_C5_Ru1	12.2		0.66	0.996	-0.001
	Period	**70.3**				

Table 1 Table of input parameters for a model of a Ru/Si ML coating with 20 bilayers and with 10 Å thick B_4C barrier layers on the top of each internal Ru and Si layer with layer thicknesses and atomic compositions determined from the elemental EELS profiles shown in Figure 7 and with thickness of the top-most layers and the densities of the 5 distinct layers within each bilayer period determined with SLitho simulation software by fitting to the reflectivity data shown in Figure 8.

Comparisons of measured (solid curves) and simulated (dashed curves) reflectivity versus wavelength and reflectivity at 13.5 nm wavelength versus angle of incidence are shown in Figure 8. The comparisons show that reasonable agreement between measurement and simulation has been obtained with the 5-layer model for each Ru-Si bilayer period.

3. RESULTS OF RIGOROUS SIMULATIONS

To better understand the impact of the new broader bandwidth Ru/Si ML reflector on mask 3D effects, the diffraction pupil at 0.33 NA and 4x magnification with both Quasar (σ_o 0.92/σ_i 0.452/ deg28) and Dipole Y (σ_o 0.92/σ_i 0.564/ deg68) illumination has been simulated. The simulation results described in this paper were performed using the rigorous mask 3D simulator S-Litho (Synopsys) [10] using a calibrated and verified mask model for standard Mo/Si

MLs with 40 bilayers including Mo-Si intermixing [11] and for ideal (no Ru-Si intermixing) Ru/Si MLs with 20 bilayers using the optical constants (n & k values at 13.5 nm wavelength) and for the modeled Ru/Si ML with optimum B_4C interlayers described in Section 2.2 all with 70 nm thick Ta-based absorbers and at 0.55 NA and anamorphic 4x/8x magnification [12] with Quasar and Dipole-Y illumination. The parameters for the three difference mask stacks are summarized in Table 2.

Stack No.	Multilayer	Absorber
MoSi ML	40 bilayer Mo/Si with intermixing	70 nm thick Ta-based
Ideal RuSi ML	20 bilayer Ru/Si no intermixing	70 nm thick Ta-based
RuSi ML w/ B4C	20 bilayer Ru/Si w/ B4C barriers	70 nm thick Ta-based

Table 2 Compilation of the mask stack models used for the simulations.

3.1 Rigorous Simulation Results at 0.33 NA and 4x magnification

Simulation results for the horizontal-vertical bias of a 16 nm CD trench through LS pitch at 0.33 NA and 4x magnification with Quasar illumination for the 3 different mask stacks listed in Table 2 is shown in Fig. 9. Simulation results for telecentricity error through LS pitch at 0.33 NA and 4x magnification with Dipole Y illumination for the 3 different mask stacks listed in Table 2 is also shown in Fig. 9.

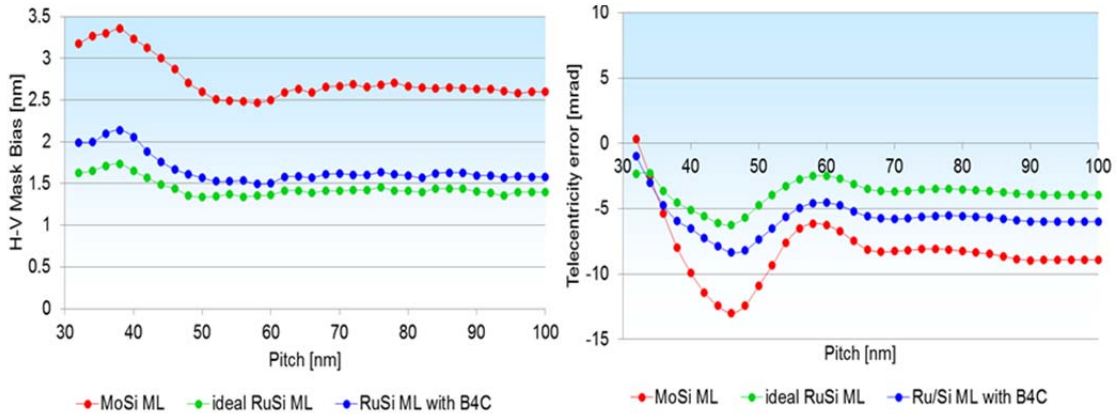

Figure 9 Left: Simulation of horizontal-vertical bias for CD 16 nm trench through L/S pitch at 0.33 NA (4x magnification) and 6° chief-ray-angle with Quasar illumination for the 3 different mask stacks listed in Table 2. Right: Simulation of telecentricity error for CD 16 nm trench through L/S pitch at 0.33 NA (4x magnification) and 6° chief-ray-angle with Dipole Y illumination for the 3 different mask stacks listed in Table 2.

The data in Figure 9 show that the Ru/Si ML reflector significantly reduces shadow bias and exhibits less pattern shift through focus than a standard Mo/Si ML. The modeled Ru/Si ML with B_4C interlayers shows similar benefits to the ideal Ru/Si ML, indicating that the shallower plane of reflection of Ru/Si ML coatings is responsible for the reduced mask 3D effects.

Simulation results for the pattern shift through focus and the overlapping process window for the printing of a two-bar trench pattern (18 nm CD, 36 nm pitch, and 250 nm length) at 0.33 NA (4x magnification) and 6° chief-ray-angle for a Mo/Si ML and for a Ru/Si ML with B_4C interlayers is shown in Figure 10.

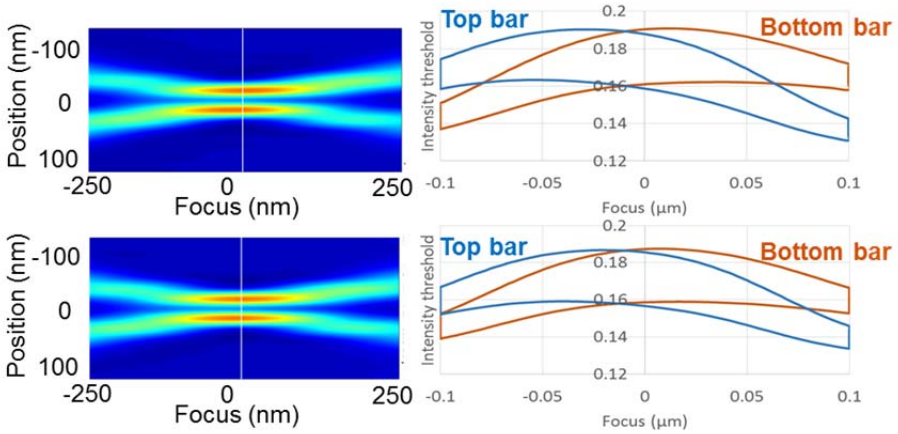

Figure 10 Simulation of Pattern-Shift and Process Window through focus of a two-bar trench pattern (18 nm CD, 36 nm pitch, and 250 nm length) at 0.33 NA (4x magnification) and 6° chief-ray-angle with Dipole-Y illumination of Mo/Si ML coatings (top) and Ru/Si ML coatings with B_4C interlayers (bottom).

The data in Figure 10 show that improved symmetry and wider overlapping process windows for the 2 bar pattern (18 nm CD trenches, 36 nm pitch and 250 nm length) can be achieved at 0.33 NA (4x magnification) and 6^0 chief-ray-angle with a Ru/Si ML with B_4C interlayer (bottom) than with a Mo/Si ML coating (top),

3.2 Rigorous Simulation Results at 0.55 NA and anamorphic 4x/8x magnification

Simulation results for the horizontal-vertical bias of 10 nm CD trench through LS pitch at 0.55 NA and anamorphic 4x/8x magnification with Quasar illumination for the 3 different mask stack listed in Table 2 is shown in Figure 11. Simulation results for telecentricity error though LS pitch at 0.55 NA and anamorpthic 4x/8x magnification with Dipole-Y illumination for the 3 different mask stacks listed in Table 2 is also shown in Figure 11.

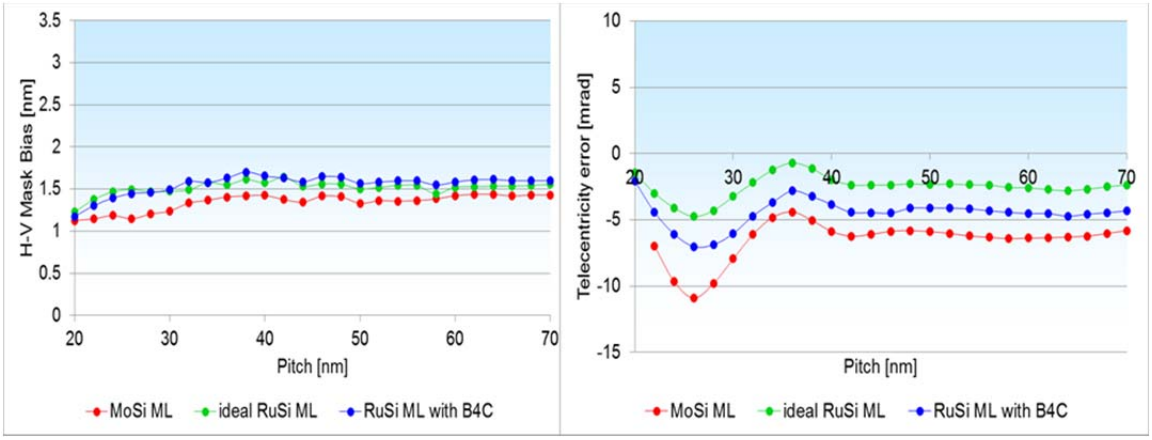

Figure 11 Left: Simulation of horizontal-vertical bias for a 10 nm CD trench through LS pitch at 0.55 NA (anamorphic 4x/8x magnification) with Quasar illumination for the 3 different mask stacks given in Table 2. Right: Simulation of telecentricity error for 10 nm CD trench through LS pitch at 0.55 NA (anamorphic 4x/8x magnification) with Dipole Y illumination for the 3 different mask stacks given in Table 2.

The data plotted in Figure 11 shows that the ML apodization is smaller for the standard Mo/Si ML than for either of the Ru/Si MLs even with anamorphic magnification causing the H-V bias versus pitch behavior at 0.55 NA and anamorphic 4x/8x magnification to be similar for Mo/Si and Ru/Si MLs. But the pattern shift through pitch (telecentricity error) performance at 0.55 NA and anamorphic 4x/8x magnification shown in Figure 11 exhibits the same trend as at 0.33 NA

and 4x magnification, namely, the performance of ideal Ru/Si MLs is better than that of modeled Ru/Si MLs is better than that of Mo/Si MLs.

Simulation results for the pattern sift through focus at the overlapping process window for the printing of a two-bar trench pattern (12 nm CD, 22 nm pitch, and 250 nm length) at 0.55 NA and anamorphic 4x/8x magnification for a Mo/Si ML and for a Ru/Si ML with B_4C interlayers is shown in Figure 12.

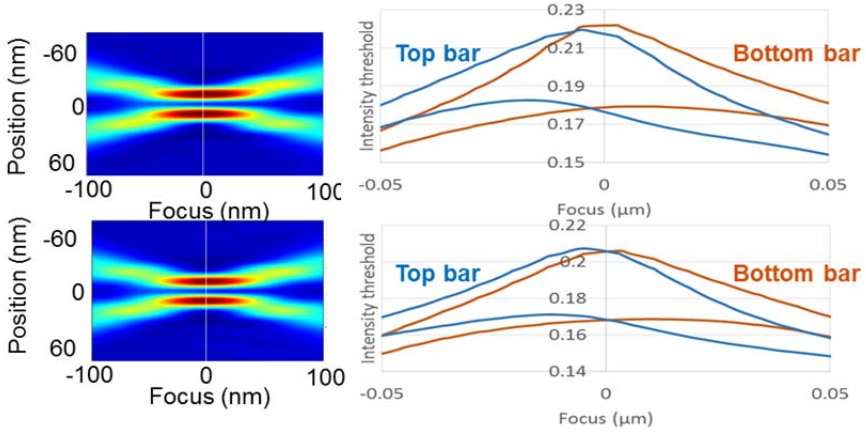

Figure 12 Simulation of Pattern-Shift through focus (left) and Process Window (right) of a two-bar trench pattern (12 nm CD, 22 nm pitch, and 250 nm length) at 0.55 NA (anamorphic 4x/8x magnification) with Dipole-Y illumination of Mo/Si ML coatings (top) and Ru/Si ML coatings with B_4C interlayers (bottom).

The data plotted in Figure 12 shows that improved symmetry and wider overlapping process windows for a 2 Bar pattern (12 nm CD, 22 nm pitch and 250 nm length) can be achieved when imaging at 0.55 NA and anamorphic 4x/8x magnification with Dipole-Y illumination with Ru/Si ML coatings with B_4C interlayers than with standard Mo/Si ML coatings.

4. CONCLUSIONS & SUGGESTIONS FOR FUTURE WORK

Non-telecentric illumination of the reflective mask in an EUV lithography tool leads to a variety of 3D mask effects including horizontal-vertical print differences, a diffraction imbalance in the pupil, and through-focus pattern placement (telecentricity) errors on the printed wafer. In this paper, we have shown that Ru/Si ML reflective coatings may be a viable alternative to the Mo/Si ML coatings that are in common use today because the lower index of refraction of Ru compared to Mo causes the effective reflective plane in Ru/Si ML coatings to be closer to the ML surface resulting in less severe mask 3D effects. We have shown that the peak reflectivity and reflective bandwidth of state-of-the-art Ru/Si ML coatings can be significantly improved by adding B_4C interlayers to reduce Ru-Si interdiffusion and improve the coating performance, but the overall performance of the Ru/Si ML coatings is still inferior to the predicted performance of ideal Ru/Si ML coatings. In conclusion, we have used rigorous simulations to show that mask stacks comprised of the broader bandwidth Ru/Si ML reflector will significantly reduce mask 3D effect on wafer imaging because the reduced intensity apodization and shallower plane of reflection leads to significantly smaller mask shadow effects, smaller pattern shifts through focus and smaller CD asymmetry and wider process window when printing horizontal 2-bar patterns with current 0.33 NA (4x magnification) EUV exposure tools and with future 0.55 NA (anamorphic 4x/8x magnification) EUV exposure tools. Future work will include the evaluation of the printing performance of an EUV mask with a Ru/Si ML reflective coating in a 0.33 NA EUV scanner.

5. ACKNOWLEDGEMENTS

The authors would like to thank Mandeep Singh of Newport Corporation for pointing out to us the advantages of Ru/Si multilayer coatings. The authors would also like to thank Scott Zaffini of JX Nippon Mining & Metals for supplying the targets needed to fabricate the ML samples. Lastly, we gratefully acknowledge the encouragement and support of Eric Hendrickx of IMEC and Professor Marc Heyns of KU Leuven.

REFERENCES

[1] Philipsen, V., Hendrickx, E., Jonckheere, R., Vanderberge, G., Davydova, N., Fliervoet, T., Neumann, J.T., "Inpact of mask stack on high NA EUV imaging," International Symposium on Extreme Ultraviolet Lithography, Brussels, Belgium (2012).

[2] Neumann, J.T., Graupner, P., Kaiser, W., Garreis, R., Geh, B., "Interaction of 3D mask effects and NA in EUV lithography," Proc. SPIE **8522**, 852211 (2012).

[3] Stearns, D., Rosen, R., Vernon, S., "High-performance multilayer mirrors for soft x-ray projection lithography," Proc. SPIE **1547**, 2 (1992).

[4] Windt, D., Hall, R., Waskiewicz, W., "Interface imperfections in metal/Si multilayers," J. Appl. Phys. **71**, 2675 (1992).

[5] CXRO X-ray database, http://henke.lbl.gov/optical-constants/

[6] Wood, O., Raghunathan, S., Mangat, P., Philipsen, V., Luong, V., Kearney, P., Verduijn, E., Kumar, A., Patil, S., Laubis, C., Soltwisch, V., Scholze, F., "Alternative materials for high numerical aperture extreme ultraviolet lithography mask stacks," Proc. SPIE **9422**, 94220I (2015).

[7] Bajt, S., Alameda, J., Barbee Jr, T., Clift, M., Folta, J., Kauffman, B., Spiller, E., "Improved reflectance and stability of Mo/Si mirrors," Proc. SPIE **4506**, 65 (2001).

[8] Bruijn, S., v.d. Kruijs, R., Yakshin, A., Zoethout, E., Bijkerk, F., "Thermally induced decomposition of B_4C barrier layers in Mo/Si multilayer structures," Surface & Coating Technology **205**, 2469 (2010).

[9] Yakshin, A., Louis, E., Gorts, P., Maas, E., Bijkerk, F., "Determination of the layered structure in Mo/Si multilayers by grazing incidence x-ray reflectometry," Physica B **293**, 141 (2000).

[10] http://www.synopsys.com/Tools/Manufacturing/MaskSynthesis/Pages/Sentaurus-Lithography.aspx.

[11] Philipsen, V., Hendrickx, E., Jonckheere, R., Davydova, N., Fliervoet, T., Neumann, J. T., "Actinic characterization and modeling of the EUV mask stack," Proc. SPIE **8886**, 888619 (2013).

[12] Migura, S., Kneer, B., Neumann, J. T., Kaiser, W., van Schoot, J., "EUV lithography optics for sub 9 nm resolution," Oral presentation at the International Symposium on Extreme Ultraviolet Lithography, Washington, D.C., Oct. 29, 2014.